Materials Today Bio 22 (2023) 100770

Contents lists available at ScienceDirect

Materials Today Bio

journal homepage: www.journals.elsevier.com/materials-today-bio

Development of a novel NiCu nanoparticle-loaded polysaccharide-based hydrogel for 3D printing of customizable dressings with promising cytotoxicity against melanoma cells

Laura Činč Ćurić [a,1], Maša Šuligoj [a,1], Maja Ibic [a,1], Nina Marovič [a,1], Boštjan Vihar [a,b], Matej Vesenjak [c], Polona Dobnik Dubrovski [c], Nejc Novak [c], Janja Stergar [c], Irena Ban [c], Uroš Maver [a,d], Marko Milojević [a,d,*], Tina Maver [a,d]

[a] University of Maribor, Faculty of Medicine, Institute of Biomedical Sciences, Taborska Ulica 8, SI 2000 Maribor, Slovenia
[b] IRNAS Ltd., Limbuška Cesta 76b, SI 2000 Maribor, Slovenia
[c] University of Maribor, Faculty of Mechanical Engineering, Smetanova 17, SI-2000 Maribor, Slovenia
[d] University of Maribor, Faculty of Medicine, Department of Pharmacology, Taborska Ulica 8, SI-2000 Maribor, Slovenia

ARTICLE INFO

Keywords:
Nanoparticle-loaded hydrogels
3D printed dressings
Polysaccharides
Nickel-copper nanoparticles
Cytotoxic activity

ABSTRACT

Polysaccharide hydrogels and metal alloy nanoparticles have already found use in a range of biomedical applications. Nickel-copper nanoparticles (NiCu NPs) are particularly promising due to their tunable properties, such as ferromagnetism, biocompatibility, and antimicrobial activity. At the same time, polysaccharide hydrogels made of polymer mixtures such as alginate and methylcellulose with incorporated metal alloy nanoparticles are reported in the scientific literature. In view of this, in this work, NiCu NPs are combined with polysaccharide hydrogels and 3D printed to construct geometrically customizable dressings with tailorable properties for melanoma treatment. This novel combination exploits the intrinsic magnetic properties of NiCu NPs and the same time builds on their less known properties to improve the mechanic stability of 3D printed materials, both contributing to a previously not reported application as potent cytotoxic dressing against melanoma cells. The dressings were evaluated in terms of their physico-chemical characteristics, and their potential application, namely melanoma cell cytotoxicity. While all dressings exhibited similar degradation profiles regardless of composition, the addition of NiCu NPs had an effect on the hydrophilicity, swelling rates, and topographical properties of the dressings. Compression results showed that the presence of NPs increased the stiffness of the dressings, while the ultimate tensile strength was highest at 0.31 MPa for the dressings with 0.5 wt% NPs. We show that although the base formulation of the dressings is biocompatible with skin-derived cells, dressings loaded with NPs exhibit promising antimelanoma activity. Extracts obtained from dressings containing 0.5 wt% NPs reduced melanoma cell viability to 61% ± 11% and 40% ± 2% after 24 h and 72 h of soaking, respectively. Furthermore, extracts of dressings with 1 wt% NPs reduced melanoma cell viability to less than 15% within the first 24 h. By adjusting the NP content, the mechanical properties, surface roughness, and wettability can be tuned so that the dressings can be functionally customized. In addition, by using 3D printing as a fabrication process, the shape and composition of the dressings can be tailored to the patient's needs. The dressings also remained intact after soaking in simulated physiological solution for 14 days, indicating their suitability for long-term topical application.

* Corresponding author. University of Maribor, Faculty of Medicine Institute of Biomedical Sciences and Department of Pharmacology Taborska ulica 8, SI-2000 Maribor, Slovenia,
E-mail address: marko.milojevic1@um.si (M. Milojević).
[1] These authors contributed equally to the article and share the first authorship.

https://doi.org/10.1016/j.mtbio.2023.100770
Received 6 February 2023; Received in revised form 31 July 2023; Accepted 10 August 2023
Available online 11 August 2023

1. Introduction

A variety of biomedical applications have already made use of polysaccharide hydrogels and metal alloy nanoparticles, especially for tissue engineering and regenerative medicine [1–5]. In addition to good biocompatibility, polysaccharide-based polymers such as alginate and cellulose derivatives have proven to be suitable materials for the preparation of reversibly crosslinkable hydrogels with tunable stiffness, swelling and degradation, which are suitable for additive manufacturing [4–10]. Nickel–copper nanoparticles (NiCu NPs) are particularly interesting for biomedical applications due to their simple synthesis, chemical stability, tunable magnetic properties, biocompatibility, and antimicrobial properties. Moreover, they exhibit tunable Curie temperature (T_C) in the therapeutic range (42–46 °C), which makes them promising candidates for use in magnetic hyperthermia (MH) [11,12]. By synthesizing polyethylene glycol-coated NiCu NPs with a T_c of ~46 °C and a saturation magnetization of 6–8 emu/g, Chatterjee et al. were the first to confirm the potential of NiCu NPs for use in MH for cancer treatment [13]. Furthermore, Kuznetsov et al. showed that by varying the composition of NiCu NPs and their synthesis parameters, NPs with T_C in a range suitable for local hyperthermia could be prepared. Testing the prepared NPs on a rat liver tumor model showed their potential use as mediators of MH [14]. Recently, Amrollahi et al. also proved their potential for use in MH, by preparing $Ni_{0.5}Cu_{0.5}$ NPs with a measured T_C of 44 °C. Biocompatibility was confirmed at low concentrations by analyzing their effect on human bone marrow stem cell proliferation [15].

Importantly, NiCu NPs also exhibit other advantageous properties, such as high drug loading capacity, potential magnetic guidance, and tracking as well as controlled drug delivery by external triggering, making them promising candidates for various multimodal therapeutic approaches, especially in cancer [16]. For example, Stergar et al. prepared a novel controlled drug delivery system based on $Ni_{67.5}Cu_{32.5}$ NPs in a silica matrix to deliver a fluorescent model drug (rhodamine 6G) to various human cells (human fibroblasts, HeLa, Caco-2). Biocompatibility and cytotoxicity tests on human fibroblasts showed that the developed system is safe for application on human skin. Considering the already demonstrated suitability T_C of such a composition, these results suggest that NiCu NPs are also promising for multimodal cancer therapies combining magnetic hyperthermia and controlled drug delivery [17].

Despite their potential, the use of NiCu NPs, particularly in tissue engineering, is still a relatively unexplored field. Recently, our group has shown that NiCu NPs can be an effective tool to control the viscosity of hydrogels, the swelling and degradation properties of scaffolds and fine-tune their topographic and mechanical properties. We have shown that NiCu NPs are also useful for *in vitro* modelling applications, as they can develop scaffolds that accurately mimic the microenvironment of healthy and pathologically altered tissues. However, this study did not investigate the therapeutic application of NiCu NPs [2]. Incorporating NiCu NPs to modify the mechanical and chemical properties is a relatively simple yet highly controllable process. When combined with spatially controlled deposition (using 3D printing) of structurally diverse materials thus has significant potential for developing novel and personalized treatment options. The possibility of locally suppressing cancerous tissue growth while stimulating the growth of adjacent healthy cells could dramatically improve treatment outcomes for patients, especially in oncology. Based on the above properties of NiCu NPs and the advantages of 3D printing, we now hypothesize that advanced polysaccharide-based dressings with target-specific geometries can be fabricated to provide antimelanoma activity only on cancer cells and adjacent wound healing properties for surrounding healthy tissue.

Thus, in the present study, we incorporated different concentrations of NiCu NPs into a newly developed polysaccharide-based formulation used for three-dimensional (3D) printing of dressings with antimelanoma properties. The effects of the NPs on the properties of the dressings were systematically investigated using advanced material characterization techniques. First, the dressings' morphology, composition, and surface properties were evaluated using atomic force microscopy, scanning electron microscopy in conjunction with energy dispersive X-ray spectroscopy, and state-of-the-art nanocomputed tomography. The general performance-related properties of the dressings were determined by hydrophilicity and swelling/weight loss measurements, and the mechanical properties were evaluated by compression and tensile tests. Finally, the biocompatibility of the dressings was determined on human skin keratinocytes and fibroblasts, and the cytotoxic antimelanoma properties were confirmed on a malignant melanoma cell line using the MTT assay. Based on a thorough literature review, we can claim to be the first to have prepared a hydrogel with embedded NiCu NPs, exploiting, simultaneously, their intrinsic properties (magnetic properties, use as a delivery system, etc.) and such that have not yet been exploited (e.g. improving the mechanical properties). Both types of properties led to the development of a completely new type of application as a patch with a potent cytotoxic effect in a specific type of cancer. The promising results of this study should lead to the development of new customizable dressings with potential cytotoxic activity against melanoma cells.

2. Materials and methods

2.1. Materials purchased and used in the preparation of hydrogel dressings

The sodium salt of alginic acid (Mw = 120–190 kDa, mannuronic to guluronic ratio = 1.56, serial number: 180,947)) and methylcellulose (MC; Mw: 17 kDa, average viscosity = 25 cP, degree of substitution 1.5–1.9, serial number: M6385) for the dressing preparation were purchased from Sigma-Aldrich, Germany. Cellulose nanofibrils suspension (NFC, 3% (w/v), 1.0 g/cm^3 aqueous gel, nominal fiber width of 50 nm and length of several hundred microns) was purchased from The Process Development Center, University of Maine (Orono, Maine, USA). All materials were used as purchased with no further modifications. In addition, ultra-pure water (18.2 mΩ cm at 25 °C) from the ELGA Purelab water purification system (Veolia Water Technologies, UK) was used to prepare all solutions. $Ni_{67.5}$ $Cu_{32.5}$ nanoparticles (NPs) in a silica (Si) matrix were synthesized using the sol-gel method described previously [18]. The method included a step of thinning the silica layer on the surface of the NPs, which renders them potentially more toxic (a requirement in this study in relation to their targeted antimelanoma activity) compared to the same NPs with thicker silica coatings. Transmission electron microscopy (TEM) was performed on the as-prepared NiCu NPs in silica, which are shown as part of the supplementary document (see the *Supplementary document* – Figure S1 for further details regarding these results).

2.2. Hydrogel preparation and 3D printing of dressings with incorporated NPs

Four different hydrogel formulations were prepared for 3D printing of the dressings; the base hydrogel formulation consisted of 10 wt% MC, 5 wt% ALG, and 1.5 wt% NFC in ultra-pure water. As a polysaccharide with carboxylic groups in its structure, ALG was chosen due to the intrinsic property of carboxylated polymers, which form firm gels in the presence of divalent ions [19,20]. MC and NFC were used mainly to increase the strength and structural integrity of the final gel. Whereas MC can importantly affect the viscosity of the gel, NFC, due to its fibrillar structure, can contribute to the final material's mechanical stability. It is worth mentioning that all three polymers are biocompatible [21,22]. To distinguish between this base formulation, which was prepared without NPs, from the following hydrogels, this formulation is from here on termed "Without NPs".

The other 3 hydrogels had the same composition as the base

formulation (10 wt% MC, 5 wt% ALG, and 1.5 wt% NFC) with additionally incorporated NPs in different amounts. The names of these hydrogels were defined according to the amount of added NPs as the percentage of the total weight of the hydrogel formulation (0.1 wt% NPs, 0.5 wt% NPs and 1 wt% NPs, respectively). NPs were weighed and mixed to the prepared formulations. The prepared gels with and without NPs were passed through a stainless-steel roller mill (Exakt 50L, Exakt Advanced Technologies GmbH, Norderstedt, Germany; 1 μm distance between rollers) to obtain a homogeneous gel. A pneumatic Vitaprint printer (IRNAS, Slovenia) with extrusion nozzles (Nordson EFD, USA) with a diameter of 0.25 mm was used for 3D printing. The geometry of the printed dressings was set to a cylindrical shape with 20 mm diameter and 1.2 mm height. The pressure was regulated during printing to obtain the optimal filament/pore size. The g-code was created using a custom-built scaffold generator, which is part of the Vitaprint software (PlanetCNC TNG v2, Slovenia). After printing, the dressings were crosslinked by complete immersion in 5 wt%. $SrCl_2$ for 60 min. We utilized $SrCl_2$ as an ionic crosslinker owing to its specific properties, which were found to be superior for this application compared to the commonly used crosslinkers such as $CaCl_2$ [23]. Sr^{2+}-crosslinked scaffolds demonstrate higher compressive strength, faster swelling, slower degradation, and a rougher surface [23]. These characteristics enhance the mechanical stability and the longevity of the dressing, potentially improving cell attachment and the interaction with melanoma cells. Sr^{2+} crosslinking can also promote higher metabolic activity, indicating a stronger biological response, while being gentle on cells, facilitating stable cultures for 30 days. Sr^{2+} also enables to adjust the scaffold properties more flexibly, aligning with our aim of precise customization. After crosslinking, the dressings were then frozen at −80 °C and lyophilized overnight at −101 °C (VirTis BenchTop 6K, SP Industries Inc., Warminster, PA, USA).

2.3. Characterization of 3D printed dressings

2.3.1. Atomic force microscopy

The topographical and surface roughness analysis of dressing formulations was performed with an atomic force microscopy setup (AFM) in tapping mode (Keysight 7500 AFM multimode scanning probe microscope, Keysight Technologies, USA). Samples for AFM measurements were prepared by pressing the hydrogels between two silicon wafers and removing them after drying. The images were scanned using silicon cantilevers (ATEC–NC–20, Nanosensors, Germany) with a resonance frequency of 210–490 kHz and a force constant of 12–110 Nm^{-1}. All measurements were performed at room temperature. For all samples, images of 50 × 50, 10 × 10, and 1 × 1 μm^2 were recorded with a resolution of 1024 × 1024 pixels. The Pico Image Basic 7.2 software (Keysight Technologies, USA) was used to process all images and to calculate the root mean square height of the surface (Sq) and arithmetical mean height of the surface (Sa) according to ISO 25178.

2.3.2. Scanning electron microscopy (SEM) with EDX

The surface morphology of the 3D printed dressings was analyzed using the field emission scanning electron microscope (FE-SEM) Supra 35 VP (Carl Zeiss, Germany) equipped with the energy dispersive X-ray (EDX) spectrometer Ultim Max 100 (Oxford, UK). Before imaging, all freshly 3D printed dressings were frozen at −80 °C, lyophilized, and pressed onto a double-sided adhesive carbon tape (SPI 116 Supplies, USA). The NiCu NPs were ground as reported previously in Ref. [18], before being similarly pressed onto double-sided adhesive carbon tape. For imaging, as-prepared samples on the carbon tape were pressed onto aluminium stubs (Agar Scientific, UK). Before EDX analysis, the samples were sputtered with a 6 nm thick conductive Pt layer using the precision coating and etching system (PECS) - model 682 (Gatan, USA). SEM micrographs were acquired with low electron beam energy (1 kV) using a secondary electron (SE) detector at magnifications of 200 × , 50,000 × , and 100,000 × , respectively. The accelerating voltage was 2 kV. EDX elemental analysis was performed at 20 kV electron beam energy with 400 pA probe current. The EDX spectra and data quantification were processed using AZtec 5.0 software (Oxford, UK).

2.3.3. ATR-FTIR

Attenuated Total Reflectance Fourier Transform Infrared Spectroscopy (ATR-FTIR) spectra were recorded using an Agilent Cary 630 FTIR spectrometer with the diamond ATR module at a scan range of 4000–650 cm^{-1} with a step of 1 cm^{-1}. The scans were performed on three different places in 8 repetitions directly on the 3D printed dressings.

2.3.4. Internal structure analysis using nano-computed tomography

Nano-computed tomography (NanoCT) was used to assess the influence of NPs on dressings' internal structure and surface properties. Images were captured with the 3D X-ray microscope ZEISS Xradia 620 Versa (Carl Zeiss AG, Oberkochen, Germany). Before analysis, the freshly 3D printed dressings were crosslinked, frozen at −80 °C, and lyophilized. The measurements were done with a 4x objective at 40 kV and 3 W without an additional filter. Exposure time was set to 1.6 s, and binning was set to 2. These settings resulted in a voxel size of 3.16 μm. The images were reconstructed using the proprietary ZEISS Xradia TXM3DViewer v1.2.10 software (Carl Zeiss AG, Oberkochen, Germany) and analyzed using NIH image analysis software ImageJ 1.52 g (NIH, Bethesda, MD, USA).

2.4. Applicative properties of 3D printed dressings

2.4.1. Wettability

The wettability of dressings was determined using an OCA15+ goniometer system (Dataphysics, Germany) with the sessile drop method [24]. Flat samples for wettability measurements were prepared by pressing the hydrogels between two silicon wafers. Fresh and dry (dried overnight at ambient conditions) samples were analyzed by measuring static contact angles (SCA). All measurements were carried out on at least three independent sample surfaces with at least six 2 μL drops of ultra-pure water at ambient conditions (T_{room} = 21–23 °C; humidity 30–50%).

2.4.2. In vitro swelling test and degradation test

The swelling kinetics of the dressings were investigated by the gravimetric method [25]. Briefly, all printed dressings were lyophilized and weighed (initial weight, W_0). The dry dressings were immersed in 1xPBS (pH 7.4) at room temperature. Respective samples were removed from 1xPBS at predetermined time intervals, and excess liquid was removed using clean filter paper, followed by weighing. The swelling ratio at time t was calculated using equation (1):

$$\text{Swelling ratio } (\%) = \frac{Wt - Wo}{Wo} \text{x } 100\% \quad (1)$$

where, W_0 and W_t are weights of the dry and swollen dressings at fixed time intervals t, respectively.

Before the start of the *in vitro* degradation test, according to Ref. [26], freshly prepared cylinder-shaped dressings (1 cm^3) were lyophilized and then weighed (W_0). Subsequently, dry dressings were placed in 12-well plates with 2 mL 1xPBS (pH 7.4) at room temperature. At predetermined time intervals, the specimens were removed from 1xPBS, washed with deionized water three times, and lyophilized again. The dressings weight remaining was calculated according to equation (2):

$$\text{Weight remaining } (\%) = \frac{Wt}{Wo} \text{ x } 100\% \quad (2)$$

where W_0 is the initial weight of the dry dressing, and W_t is the weight of the dressing at fixed time intervals. For both tests, all measurements were executed in triplicates, and the result is reported and plotted as the

average with the corresponding standard error.

2.4.3. Mechanical properties – compression and tensile test

The compressive and tensile mechanical properties of 3D printed dressings were defined using the uniaxial testing machine Tinius Olsen H10KT (Tinius Olsen TMC, USA). Test specimens of the dressings were 3D printed as described in section 2.1 on the day of testing to preserve the quality of the materials' mechanical behaviour. The specimen size and shape were determined based on ISO 527–2:2012 type 1BB for the tension tests and ISO 604:2002 for the compression tests. The dog bone-shaped specimens with a rectangular cross-section (total specimen length: 50 mm, gauge length: 20 mm, gauge width: 4 mm, and gauge thickness: 1.5 mm) and cylindrical specimens (diameter: 10 mm and height: 10 mm) were used for determination of compressive and tensile properties, respectively. Five specimens for each material configuration and loading type were manufactured to achieve representative mechanical results. The size and shape of the used standard allowed for the feasible manufacturability of the specimens. For each material, mechanical tests were performed to define the magnitude of the force and displacement. Based on the preliminary testing and results, optimal settings for actual measurements were determined. The load cell with a maximum loading force of 50 N was used for the detailed characterization of soft testing materials. For the actual measurements, three specimens for each material configuration were tested and checked to confirm repeatability.

2.4.4. Safety (through fibroblast and keratinocyte cell viability) and efficiency (through melanoma cell cytotoxicity) testing

All cell viability assays were performed using human skin-derived cells, namely commercially available skin fibroblasts (ATCC CCL-110™, Detroit 551, LGC Standard, United Kingdom), a malignant melanoma cell line (ATCC CRL-1619™ A-375, LGC Standard, United Kingdom) and an aneuploid immortalized keratinocyte cell line from adult human skin (HaCaT). The latter were kindly provided by Prof. Dr. Elsa Fabbretti (Centre for Biomedical Sciences and Engineering, University of Nova Gorica, Slovenia). The influence of different 3D printed dressings on cell viability was evaluated via the reduction reaction of the tetrazolium salt MTT (3 (4,5 dimethylthiazolyl-2)-2,5-diphenyltetrazolium bromide), purchased from Sigma Aldrich, Germany. This is a widely accepted and reliable method for examining metabolic activity as a proxy indicator of cell viability [27,28]. In this study, the MTT assay was performed according to Mosmann [29], and the sample extraction was carried out according to ISO 10993-5 and ISO 10993-12 regulations. Briefly, lyophilized 3D printed cylinder-shaped dressings (diameter 20 mm; height 1.2 mm) were sterilized on both sides under UV light for 30 min and soaked into 2 mL of Advanced Dulbecco's Modified Eagle's Medium (ADMEM; ThermoFisher, Germany) for melanoma cells and fibroblasts/2 mL ADMEM F12 for HaCaT supplemented with 5 v/v % Foetal Bovine Serum (FBS; ThermoFisher, Germany), and incubated for 24 h or 72 h at 37 °C in an atmosphere containing 5 wt% CO_2. The malignant melanoma cells, skin fibroblast cells and keratinocytes (10.000 cells/well) were seeded into a 96-well microtitre plate with a final volume of 100 μL of ADMEM/ADMEM F12 medium supplemented with 5 v/v% FBS per well. All cells were exposed to the same volume (100 μL) of the as-prepared respective sample extracts, and their dilutions of 1:2, 1:4, and 1:8, followed by incubation for 24 h at 37 °C in an atmosphere containing 5 wt% CO_2. After incubation, 10 v/v% MTT reagent prepared in ADMEM/ADMEM F12 was added to the wells (100 μL per well). After 3 h, the medium was discarded, and the purple crystals were dissolved in DMSO. The absorbance was measured at 570 nm using Varioskan Multiplate Reader (ThermoFisher Scientific, Germany). Control cells were incubated only in their respective media. No IC_{50} values are reported since the goal was to eradicate the melanoma cells completely. All experiments were performed in four parallels, and the results are shown as average values with corresponding standard deviations.

2.5. Statistical analysis

All numerical values are reported as mean ± standard deviation (SD). The Shapiro-Wilk test confirmed the normal distribution of experimental data. Levene's test was used to assess the equality of variances. As all data sets were well-modelled by a normal distribution and homoscedastic, a one-way analysis of variance (ANOVA) followed by the Bonferroni post-hoc test was carried out accordingly. Obtained p-values <0.05 were considered statistically significant. Statistical analysis was performed using SPPS Statistics 27 (IBM Corp. Armonk, NY, USA).

3. Results and discussion

3.1. Characterization of 3D printed dressings (composition, surface, and internal morphology)

The surface morphology and porosity of the dressings were evaluated using SEM (Fig. 1A) and AFM (Fig. 2A). Scanning electron micrographs show the presence of salt crystals, probably excess $SrCl_2$ and NaCl, formed by the substitution between crosslinking agent and Na-alginate solution, which was confirmed by EDX (Fig. 1B) analysis. SEM determined no significant differences in surface properties between samples. However, nanoparticles were visible at 100.000x magnification in the dressing containing 1% NiCu. They were seen as small dots that homogeneously covered the entire surface. When an image was taken using the line integration method at 100.000x magnification, the resulting high-energy electron beam disturbed the surface, so a snapshot was taken, resulting in a lower-resolution image. The overall sample morphology of the 3D printed materials was as expected for polymeric materials with no special surface features and clearly visible 3D printed filaments. The latter seem to become thinner with increasing NP concentration (upper row at 200x magnification). With increasing magnification, further specific sample-related features appeared. For example, while the sample without NPs shows a more porous structuring of the surface, is the latter almost invisible for the sample with the highest NP content (1 wt% NP). Such behavior was also observed in previous studies, where more compact and less porous filaments of 3D printed materials were reported when the content of included NPs increased [2]. The sizes of the visible pores for the samples decrease with the NP content from a range of several hundred microns for the sample without NPs to almost no visible pores for the sample 1 wt% NP. Since our aim was not to produce materials for skin regeneration, which would necessitate bigger pores (as the ones seen in the sample without NPs), but to prepare dressings for melanoma treatment, such surface properties are acceptable. Furthermore, considering the proposed scenario of tailoring the dressing by having a more heavily loaded part with NPs intended to be in contact with the melanoma lesion in the center and an NP-less part on the exterior of such a dressing, such surface properties might even support an ideal treatment option. Namely, the interior, with its compact structure, can directly affect the lesion with high effectiveness (an increased contact surface resulting from the compactness), whereas the exterior can even promote cell growth into the cavities present in the material, boosting the healing capacity.

During SEM analysis, the composition of the dressings was evaluated by EDX at 200 × magnification. The results are summarized in Fig. 1B. Samples containing 0.5 wt% or 1 wt% NPs show the corresponding elemental signals for Ni, Cu, and Si representing the NPs and confirming their presence in the materials. For the samples containing 0.1 wt% NPs or less, the concentration is below the detection limit of the method. Since discrete regions of the sample are evaluated, some deviation from the average values of the component concentrations is to be expected, which explains the non-linear change in the measured fractions compared to the expected concentrations (as determined by the preparation). Consequently, at this magnification, the distance between NPs at 0.1 wt% could be so large that particles are completely missed.

AFM revealed more details that shed light on how NPs affect the

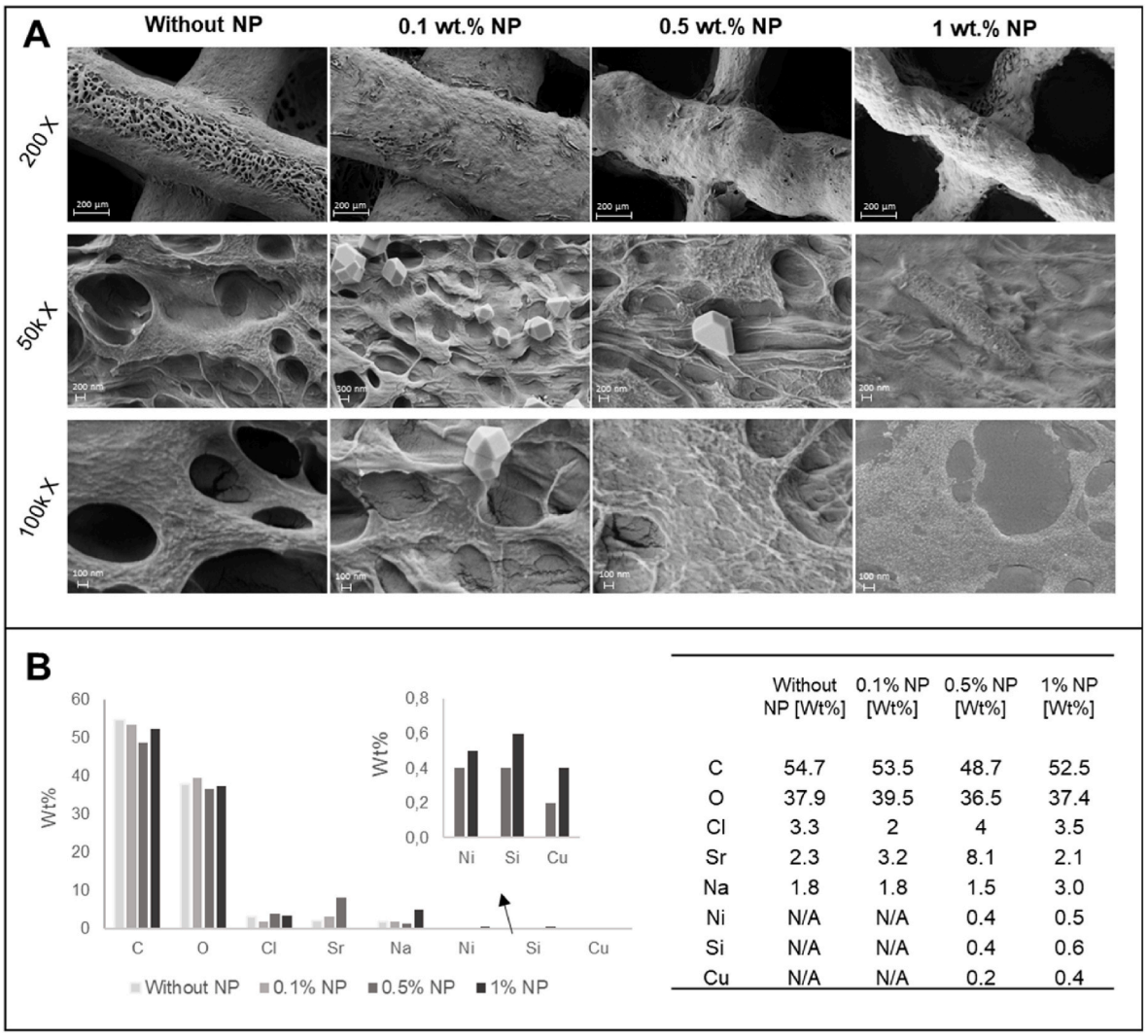

	Without NP [Wt%]	0.1% NP [Wt%]	0.5% NP [Wt%]	1% NP [Wt%]
C	54.7	53.5	48.7	52.5
O	37.9	39.5	36.5	37.4
Cl	3.3	2	4	3.5
Sr	2.3	3.2	8.1	2.1
Na	1.8	1.8	1.5	3.0
Ni	N/A	N/A	0.4	0.5
Si	N/A	N/A	0.4	0.6
Cu	N/A	N/A	0.2	0.4

Fig. 1. SEM and EDX analysis of 3D printed dressings with incorporated NiCu NPs. A) SEM images of dressings were taken at 200 × , 50.000 × and 100.000 × magnification; B) EDX compositional analysis of dressings.

surface roughness of crosslinked and lyophilized dressings. Measured on 50 × 50 μm squares, the surface root mean square height (S_q) increased from 0.227 μm for samples without NPs to 0.956 μm for samples containing 1 wt% NPs. Similarly, the arithmetic mean height (S_a) increased from 0.103 μm to 0.697 μm (when evaluating the same pair of samples). A significant increase in roughness with increasing NP concentration was also observed for the 10 × 10 μm and 1 × 1 μm scan dimensions. The increased surface roughness indicated by the increased S_q and S_a values can be attributed to the incorporation of NiCu NPs into the dressings. This could have several implications in the context of skin application. First, it may contribute to the adhesion of the dressing to the skin and provide a more stable contact interface between the dressing and the skin [30]. This may be particularly beneficial in the treatment of melanoma, as it ensures that the dressing stays in place, improving the sustained delivery of NiCu NPs. Second, the increased surface roughness may improve the interaction between the dressing and the skin microenvironment [31], potentially increasing the cytotoxicity of NiCu NPs against melanoma cells. Due to the larger surface area, the increased roughness may facilitate the interaction between the NiCu NPs and melanoma cells, thereby promoting the cytotoxic effect of the NPs. The fact that the surface roughness increased with the concentration of NPs also suggests that we can adjust the surface roughness (and thus the adhesion and interaction with melanoma cells) by adjusting the concentration of NP in the dressing. This contributes to the customizable nature of these hydrogel dressings.

NanoCT analysis was used as a complementary method to SEM and AFM, serving to elucidate not only surface characteristics, but also to reveal the internal microstructure of the dressings, notably the porosity and distribution of the NPs. The results are presented and summarized in Fig. 2. A discernible internal porosity is evident across all formulations prepared, as shown in Fig. 2B, demonstrating a level of consistency in this regard. The NiCu nanoparticles are visible as white spots within the nanoCT reconstructed images, an observation which corroborates with the anticipated increase in the number of these spots with rising nanoparticle concentrations. In fact, from these nanoCT images, it is apparent that the nanoparticles are evenly and homogeneously distributed across the bulk of the scaffold, providing a broad and consistent coverage throughout. Interestingly, as the nanoparticle concentrations increase, the formation of larger conglomerates becomes evident, approximately 10 μm in size. This observation suggests a degree of nanoparticle aggregation at higher concentrations, a phenomenon that could potentially influence the properties of the 3D printed dressings. The images were analyzed using ImageJ software to further elucidate the differences in internal microstructure and evaluate the influence of NiCu NPs on the

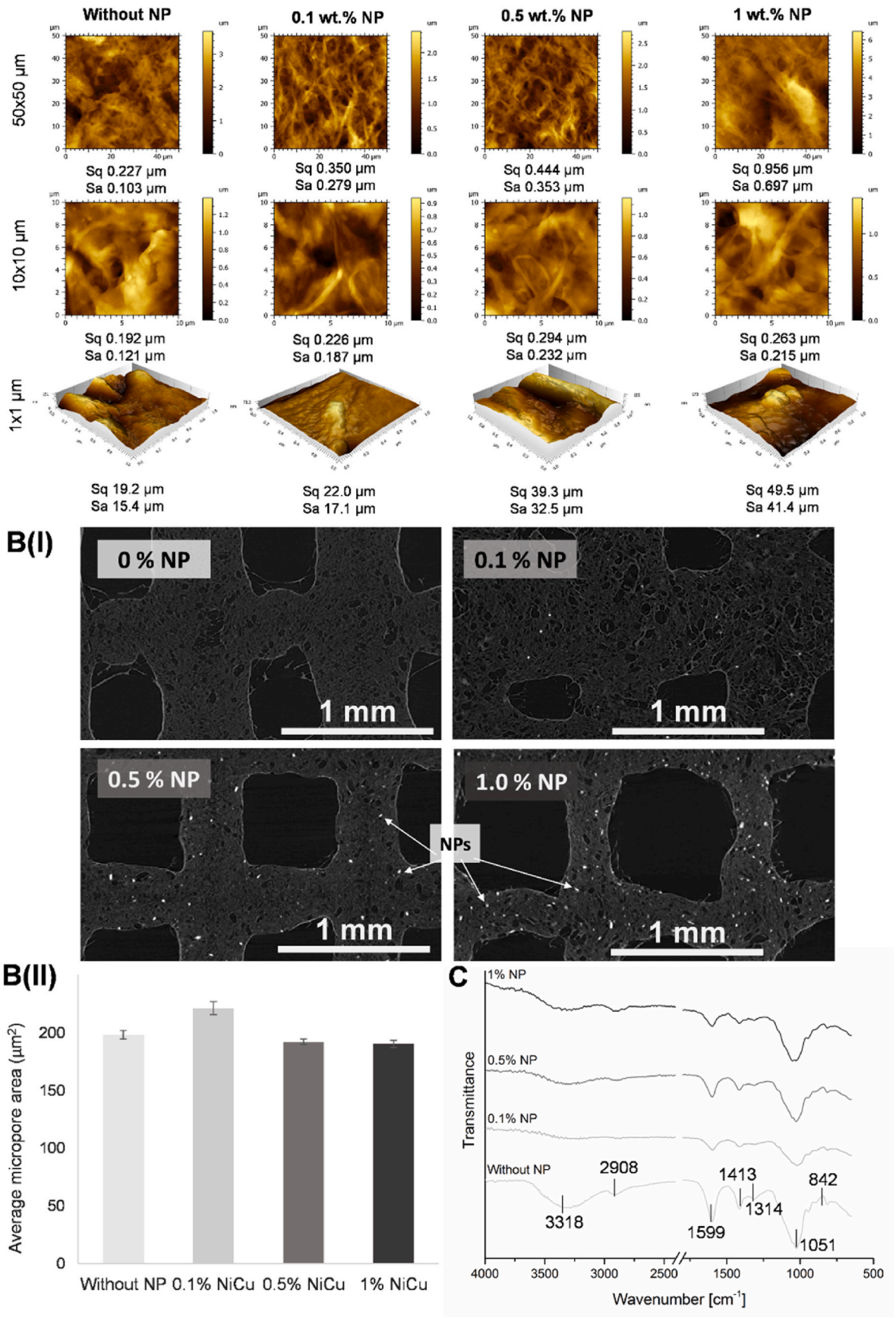

Fig. 2. A: AFM images with corresponding surface roughness parameters. B: (I) NanoCT images (II) micropore size as analyzed with ImageJ, C: ATR-FTIR spectra of dressings with highlighted peaks.

dressings. The results are shown in Fig. 2B. No significant differences exist in micropore size and overall microporosity for all dressings, regardless of composition.

In addition to the EDX analysis, which focused on elemental composition, the molecular structure of the dressings was further elucidated using ATR-FTIR. FITR spectra were obtained for all four dressings, yielding valuable information on the characteristic functional groups and chemical bonds present. The O–H stretch characteristic of the hydrogen bonds present in the polysaccharides was observed at 3318 cm^{-1}, while the C–H stretch was seen at 2908 cm^{-1}. At 1599 cm^{-1}, COO- groups, indicative of guluronic or mannuronic acid in sodium alginate, were discerned. This was assigned to the stretching of the carboxyl group, a significant component in determining the dressing's hydrophilic properties. Furthermore, the peak at 1413 cm^{-1} can be attributed to CH_2 bending due to CH_2 scissoring. This contributes to the overall structural integrity and strength of the dressings. The band at 1027 cm^{-1} corresponds to C–O stretching, indicative of either C–O–C or C–O–H groups present in NFC, MC, and ALG. These groups play a crucial role in the interaction between the dressing materials and the wound environment. NiCu nanoparticles, which were included in our dressings at different concentrations, have been reported to show peaks at 1056 cm^{-1} and 780 cm^{-1}, corresponding to symmetric and asymmetric Si–O–Si vibrations, respectively. In our study, these peaks were superimposed by the C–O stretching peak. However, as the concentration of NiCu nanoparticles was increased, the C–O stretching peak became more pronounced, indicating successful integration of nanoparticles in the dressing. Complementing these findings, our EDX results (as described in the SEM analysis) confirmed the presence of Ni, Cu, and Si in samples containing 0.5 wt% or 1 wt% NPs. This corroboration further bolsters our assertion that NiCu nanoparticles were successfully integrated into the dressing, as reflected by the enhanced C–O peak in the FTIR spectra [2].

It is also important to point out that by introducing nanoparticles into the hydrogel, the viscoelastic properties of the printing ink are changed, which results in an altered extrusion behaviour and consequently, an altered filament diameter, as shown in Figs. 1 and 2. However, as shown in Fig. 4, the shape and outer dimensions between samples are reproducible, which is essential for dressing customization and suitable for tailoring the scaffolds to melanoma's shape. In this sense, the observed variations of extruded filament do not affect the function of the scaffolds or potential dressings.

3.2. Determination of general performance-related properties of 3D printed dressings

3.2.1. Influence of NPs on dressings hydrophilicity, swelling and degradation properties

Static contact angles (SCA) of ultrapure water were measured to assess how the content of NPs affects the hydrophilicity of the respective dressings. The results are summarized in Fig. 3. As hydrogel-based structures, all fresh dressings exhibit highly hydrophilic properties, which are enhanced by the addition of NPs. The increased hydrophilicity can be attributed partly to the hydrophilic nature of the NiCu NPs [18] and partly to the increase in surface area (as a function of increased roughness, as confirmed by AFM analysis), which improves the wetting properties of the bulk material. Addition of 0.1 wt% NPs has no significant effect on the surface wettability of fresh samples, but an increase to 1 wt% NPs reduces the contact angle of water from 53.66 ± 1.97° (control sample) to 30.18 ± 3.55°.

In contrast, increasing the amount of NPs by 0.1 wt% showed a significant impact on the wettability of dry samples, reducing the average contact angle from 84.30 ± 7.88° (control) to 64.05 ± 7.85°.

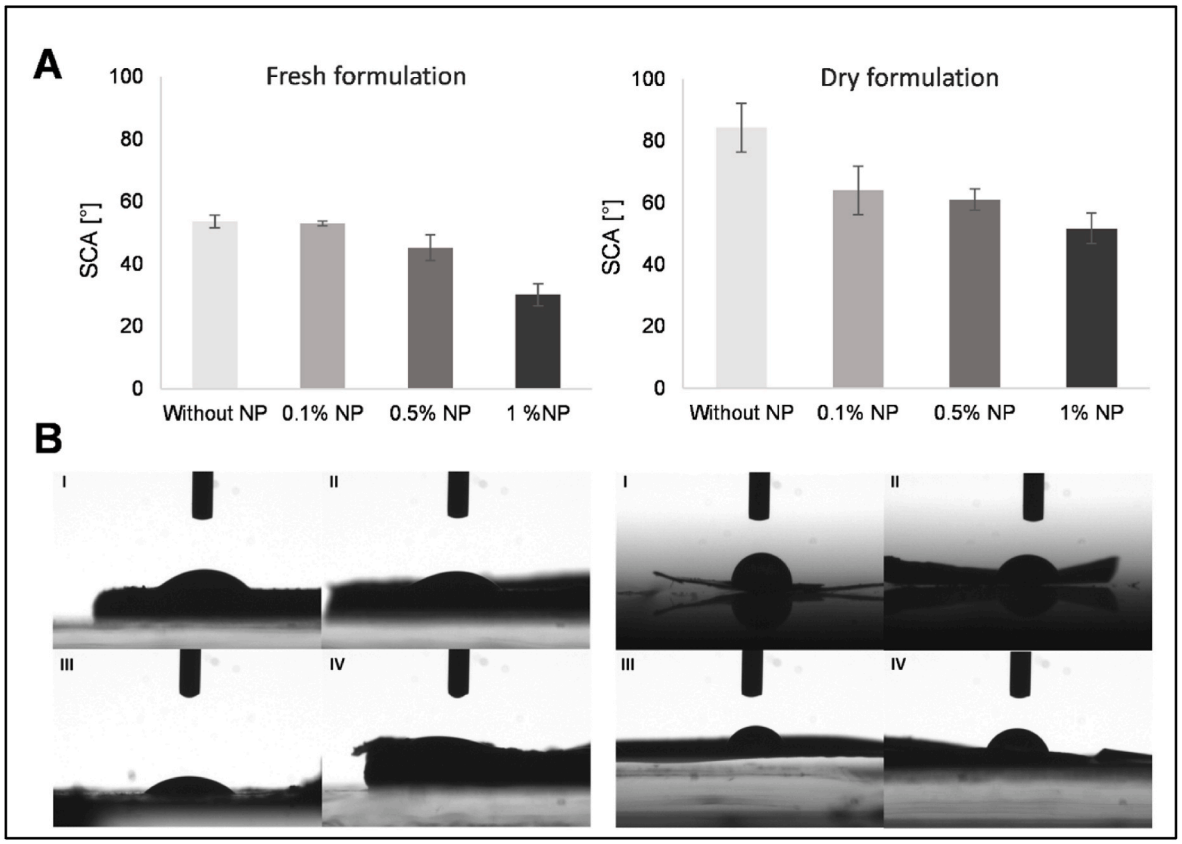

Fig. 3. Hydrophilicity of fresh and dry dressings with different NiCu concentrations. A) left: static contact angle of a freshly prepared dressing, A) right: static contact angle of a dry dressing. B) left: freshly 3D printed dressings (I: without NPs, II 0.1 wt% NPs, III: 0.5 wt% NPs and IV: 1 wt% NPs) B) right: dry 3D printed dressings ((I: without NPs, II 0.1 wt% NPs, III: 0.5 wt% NPs and IV: 1 wt% NPs).

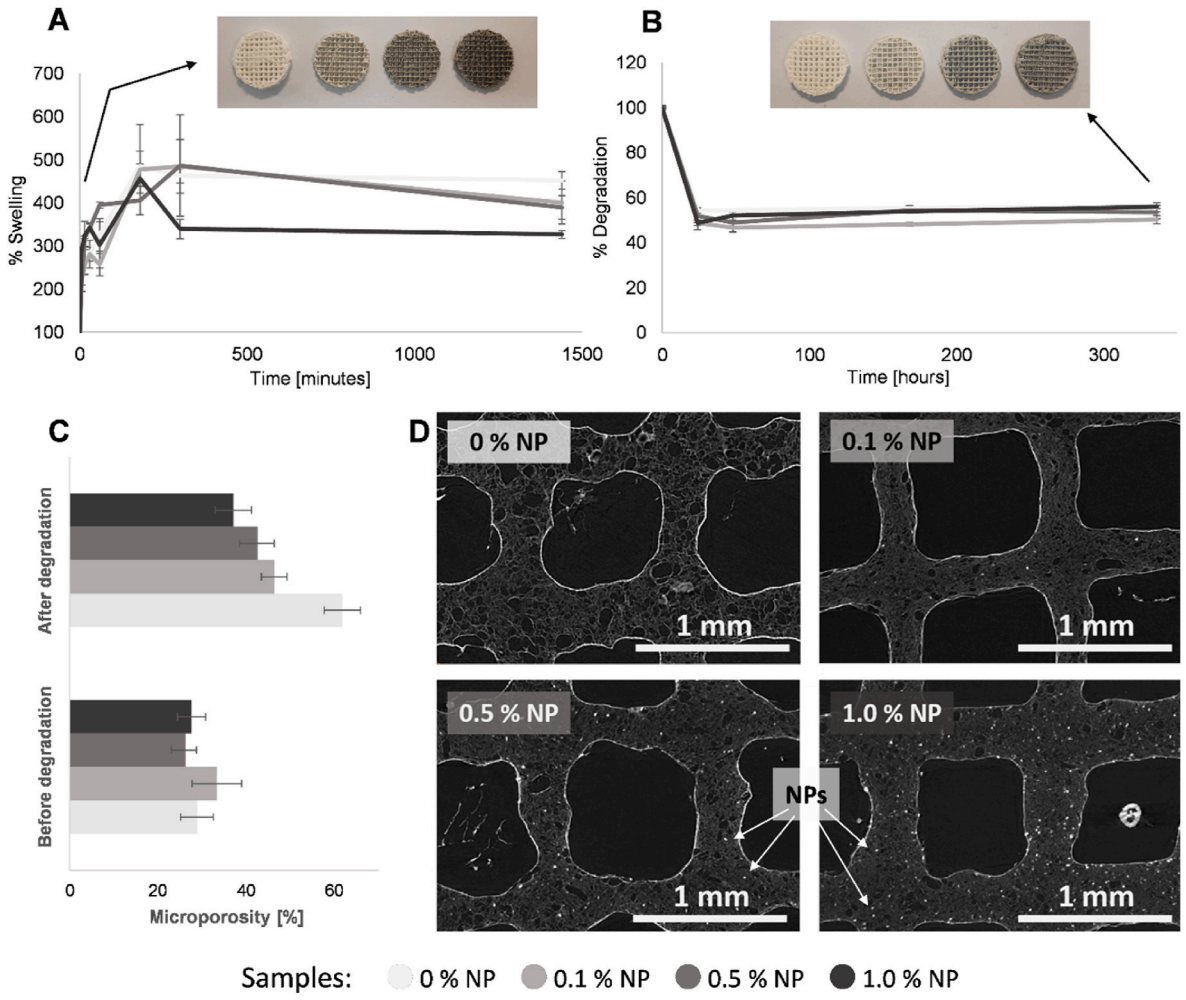

Fig. 4. A: Swelling profile of all four formulations, with a photograph of the different dressings at the start of the experiment (before swelling) B: Degradation profile of all four formulations, with a photograph of the different dressings at the start of the experiment (before swelling), C: calculated microporosity from nanoCT images before and after degradation, D: nanoCT images of dressings after degradation. The samples have been color-coded in grayscale, with each shade of grey representing NP content from lightest (0% NP) to darkest (1% NP).

Increasing the amount of NPs further lowered the contact angles, reaching 51.75 ± 4.86° at 1 wt%. This indicates that the NiCu NPs increase the wettability of the dressings both by increasing the surface area and by their intrinsically hydrophilic properties [32].

Swelling properties are an important characteristic of hydrogels, and it is not different in the context of melanoma treatment since the swelling capability can play a crucial role in their performance. For instance, it can influence the hydration state of the wound (which might be present as part of the melanoma-associated lesions) [33], the absorption of wound exudate (or any form of pus) [34], and ultimately the overall healing process. Additionally, the swelling behavior can affect the release kinetics of therapeutic agents and other incorporated active components (e.g., NPs) [35], in this case, NiCu NPs. As the hydrogel swells, it can facilitate a controlled and sustained release of the nanoparticles, ensuring an optimal concentration at the application site over an extended period. As our research employs polysaccharide hydrogels, which have well-documented swelling characteristics, this property is inherent to our materials [2,23].

The swelling behavior of the 3D printed dressings was evaluated by soaking the dried dressings in 1xPBS and determining their mass at different time intervals. The results are summarized in Fig. 4C. All dressings show an increase in total mass within the first 200–300 min after soaking, reaching an increase of 400–500% due to fluid absorption, followed by a gradual decrease in mass due to degradation. The variability of each sample contributes to the variation in results; however, no significant differences were observed between dressings.

To evaluate the degradation kinetics, the dry mass (obtained by lyophilization) of the 3D printed dressings was evaluated after a series of incubations in 1xPBS, as described in the Methods section. The results are summarized in Fig. 4D. The graph shows the relative mass retention of each dressing (compared to its initial weight) for each time point, with a curve drawn for each dressing formulation. The mass of all dressings drops rapidly during the first few hours of incubation and stabilizes after 24 h, maintaining 45–60% mass during the remainder of the incubation period. Since the dressings were incubated in a limited volume of 1xPBS, its capacity to dissolve the dressings has a limit that was reached within 24-h. The dressings are ionically crosslinked; therefore, it could be argued that increasing the volume or regularly replacing the solvent would completely disintegrate the dressings. However, the aim of this experiment was comparative degradation as a function of NPs content. All the dressings exhibited similar degradation profiles regardless of their composition, suggesting that the NiCu NPs do not contribute significantly to the degradation process. To explain the initial 50% weight loss, additional nanoCT images were acquired after the dressing degradation to analyze the internal microstructural changes. The nanoCT images showed that the internal macro- and microporosity increased significantly after degradation. Fig. 4C shows the microporosity of the dressings before and after degradation,

analyzed with ImageJ software. As shown in the graph, the increase in microporosity is highest for the dressing without NPs (28.9 ± 3.7%, before and 61.8 ± 4.1%, after degradation). The highest swelling rate was also observed for the dressing without NP, which explains the highest microporosity. The 0.1 wt% and 0.5 wt% NP dressings have similar swelling profiles, and the microporosity is also not statistically significant between the two (45.4 ± 2.9% and 42.6 ± 3.8% for 0.1- and 0.5 wt% NP, respectively). The lowest microporosity was observed for the 1 wt% NP dressing (27.6 ± 3.2% before and 37.1 ± 4.1% after degradation). In contrast to porosity, NP content has remained comparable after degradation, with the NPs still clearly visible in the nano CT reconstructions.

3.2.2. *Influence of NPs on dressings mechanical properties*

The mechanical properties of the dressings are shown in Fig. 5 with the numerical values of marked parameters summarized in Table 1. The average standard deviations of the responses for a different amount of NPs up to a strain of 0.5 were calculated and are 0.017 MPa and 0.0008 MPa in the case of compression and tensile testing, respectively.

The compression results (Fig. 5A) showed that the presence of NPs increases the stiffness of the dressings. The increase in stiffness is not so pronounced when comparing the dressings with higher amounts of NPs: 0.5 wt% and 1 wt% NPs. The mechanical responses show that the stiffness of the dressings decreases at a strains of about 0.5 for all the dressings studied, which is a consequence of the local structural failure [36]. The decrease in stiffness is followed by another increase in stiffness, with a comparable modulus to the first loading phase. The decrease in stiffness is much less significant for the dressings with 0.5 wt% and 0.1 wt% NPs, resulting in a higher load capacity at larger displacements. The strength moduli were calculated using the method schematically shown in Fig. 5 and are given in Table 1. The *E1* and *E2* moduli increased with increasing amount the NiCu NPs, while the increase is less significant at 0.5 wt% and 1.0 wt% NPs compared to the 0 wt% and 0.1 wt% NPs.

The tensile testing results (Fig. 5B) show significantly different mechanical responses than the compression tests. The tensile responses are quasi bi-linear, with stiffness decreasing at a displacement of about 0.1 for all dressings tested. The E_1 and E_2 moduli (Table 1) increased with the increasing amount of NiCu NPs in tensile loading. Stiffness and ductility (strain at failure) were highest for the dressings with 0.5 wt% NPs, with a slight decrease, observed for the dressings with 1 wt%. This suggests that in the range of 0.5 - 1 wt %, the particle-to-matrix ratio reaches the highest mechanical strength, but a further increase in NP concentration leads to a decrease in mechanical strength. This is surprising as previous studies have shown that the increase in hydrogels' mechanical strength by incorporating NPs continues well beyond 5 wt % [3,37]. The base material used in this work is already a complex composite material without adding NiCu NPs, which could explain the observed behavior. However, the available data suggest that the potential to improve the mechanical properties with NPs is high.

3.3. *Cell based tests*

Established cell lines of skin fibroblasts, keratinocytes, and malignant melanoma were deliberately selected for our *in vitro* models for two main reasons. First, their use conforms to the "3R" (Replacement, Reduction, Refinement) guiding principles for more ethical research overcoming the numerous limitations of animal models (e.g., important differences in anatomy and physiology between the animal and human skin). Second, being isolated from human skin sources, their responses to tested materials represent an essential step on the path to *in vivo* testing [38]. 3D printing allows precise customization in terms of shape and composition, thus allowing dressing personalization adapted to the shape and complexity of skin lesions or, in this instance, the melanoma's geometric features. Therefore, the experimental design for cell-based testing was structured into two parts. Testing the safety of NP-free materials (providing a supporting structure to the active part of the dressing) on keratinocytes and fibroblasts and testing the efficacy of anti-melanoma activity using NP-loaded materials (the active part of the dressing).

3.3.1. *Safety testing*

The dressings were incubated for 24 or 72 h in cell medium, and the extract was added to the cells directly or in dilutions of 1:2, 1:4, and 1:8, respectively, followed by a 24 h incubation and measurement of the overall metabolic activity using the MTT assay as a proxy for cell viability (according to ISO 10993). The results are summarized in Fig. 6A–C. The relative viability of skin fibroblasts in the undiluted, extract-rich medium was 144 ± 19% and 132 ± 7% after 24 and 72 h, respectively, and was significantly higher ($p < 0.05$) compared to control samples. A significant increase in metabolic activity was also observed using 1:2 diluted extracts at 133 ± 11% and 117 ± 6% (24 and 72 h incubation, respectively). After exposing the cells to extracts diluted to 1:4 or above, the relative metabolic activity became comparable to the control samples. HaCaT cells behaved slightly differently, with the highest increase in metabolic activity observed using diluted extracts (1:4 dilution yielded 29 ± 2% increase in metabolic activity above the control, a 1:2 dilution yielded a 28 ± 2% increase). However,

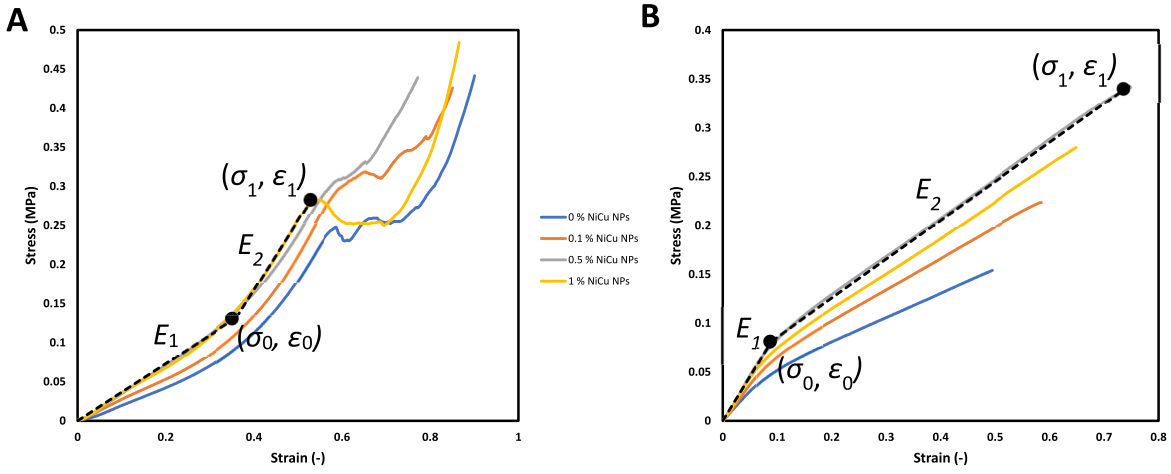

Fig. 5. Mechanical properties of the dressings. A compression, B tensile mechanical responses with the schematical determination of strength moduli *E1* and *E2* with characteristic points.

Table 1
The strength moduli E1 and E2 and characteristic points, given in the following units: E [MPa], ε [−], σ [MPa]). Plotted in Fig. 5A (compression results) and 5B (tensile results).

	Compression						Tensile					
	E_1	ε_0	σ_0	E_2	ε_1	σ_1	E_1	ε_0	σ_0	E_2	ε_1	σ_1
0% NiCu NPs	**0.22**	0.36	0.08	**0.76**	0.59	0.25	**0.56**	0.09	0.06	**0.25**	0.50	0.16
0.1% NiCu NPs	**0.28**	0.37	0.11	**0.87**	0.59	0.30	**0.70**	0.10	0.07	**0.32**	0.65	0.25
0.5% NiCu NPs	**0.37**	0.37	0.14	**0.89**	0.53	0.29	**0.91**	0.09	0.08	**0.40**	0.65	0.31
1% NiCu NPs	**0.37**	0.36	0.14	**0.88**	0.55	0.30	**0.84**	0.09	0.07	**0.37**	0.65	0.28

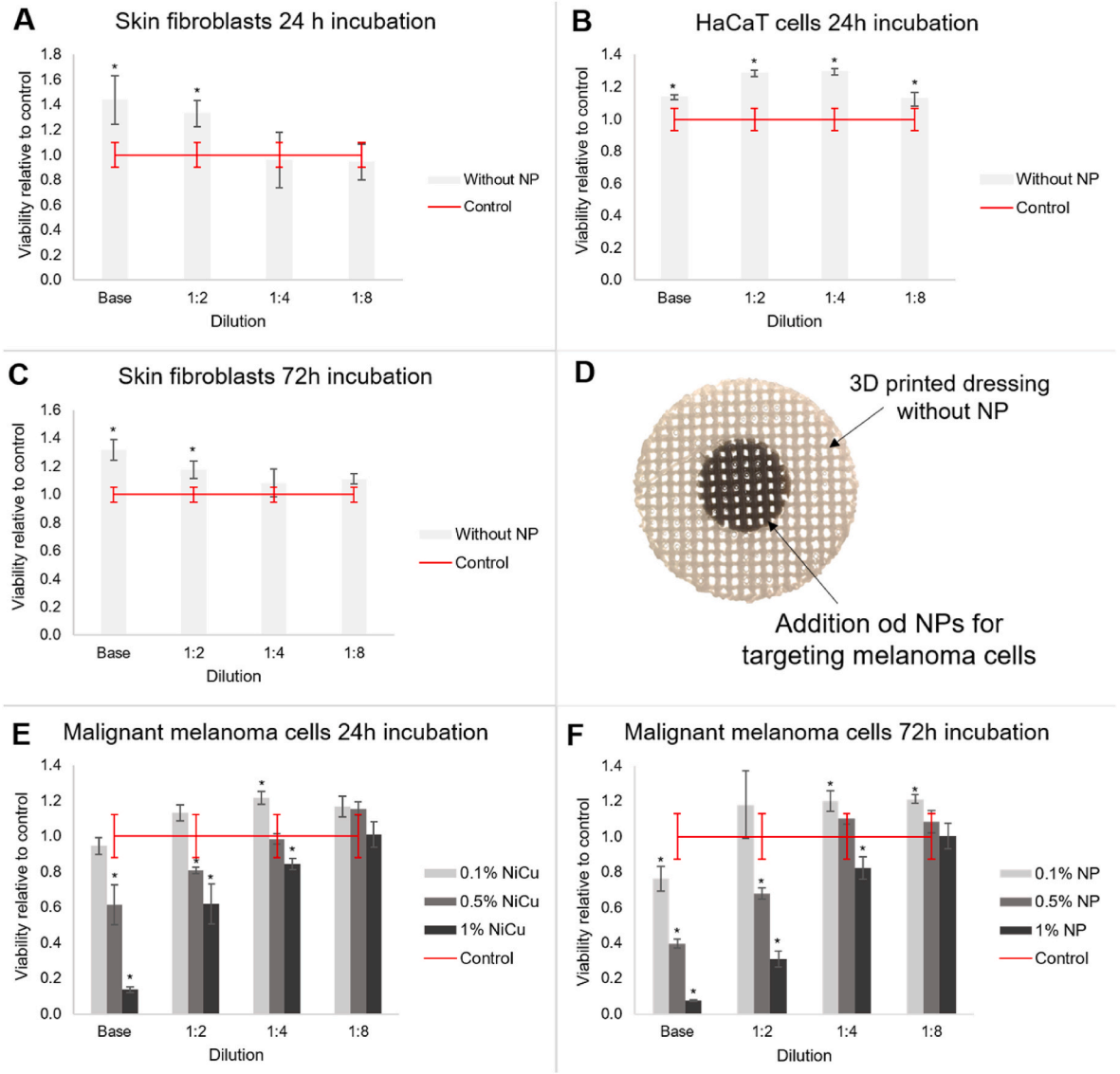

Fig. 6. Cell based testing without added NPs: A) Viability of skin fibroblasts when in contact with dressings extracts incubated in cell media for 24 h; B) Viability of skin keratinocytes when in contact with dressings extracts incubated in cell media for 24 h; C) Viability of skin fibroblasts when in contact with dressings extracts incubated in cell media for 72 h. D) The proposed tailor-made dressing for the local treatment of skin melanoma.

both the undiluted extract (13 ± 1% increase) and the 1:8 dilution (12 ± 1% increase) showed an increase in metabolic activity compared to the control. The results are shown in Fig. 6A–C.

The experiment was performed on HaCaT cells only after 24 h because they are the first cells to come into contact with the dressing (keratinocytes are the only cells in the epidermis, which is in direct contact with topical formulations on non-wounded skin). After this initial exposure, the dressing extract penetrates deeper into the skin (and into the dermis, where the skin fibroblasts are the predominant type of cells), and after 72 h, the skin fibroblasts are much more affected. Similar viabilities, regardless of the dilution of exposed HaCaT cells compared to the unexposed control, show that "peak" performance regarding the positive effect of the dressings on this type of cells can be achieved even with lower extract concentrations. These results further prove the promising nature of the developed dressings to aid skin healing/regeneration. The results indicate that NP-free materials positively affect the viability of healthy skin cells and could be used as skin-safe dressings.

3.3.2. Anti-melanoma activity

The next set of experiments was focused on evaluating the anti-melanoma activity of the NP-loaded dressings. The dressing materials described above (10 wt% MC, 5 wt% ALG, and 1.5 wt% NFC) were supplemented with nanoparticles to produce three materials with increasing final NP concentrations (0.1, 0.5, and 1 wt%). After 24 or 72 h of incubation in the cell culture medium, the 3D printed dressing extracts were tested on melanoma cells, and the results are shown in Fig. 6E and F. Fig. 6D shows an example of how 3D printing could be used to create custom-shaped anti-melanoma dressings for targeted application on patients with NP-rich material covering melanoma and NP-free material covering healthy skin. As for skin fibroblasts, the dressing was incubated in the medium for either 24 or 72 h. Addition of 0.1 wt% NPs did not drastically reduce viability in either case (94 ± 5% and 76 ± 7% at 24 and 72 h of incubation, respectively), although a negative trend in cell viability can already be noticed. Adding 0.5 wt% NPs already reduced viability to 61 ± 11% and 39 ± 2% at 24 and 72 h of incubation, respectively. Addition of 1 wt% NPs decreased the viability to 13 ± 2% at 24 h incubation and 8 ± 0.4% at 72 h incubation. The longer the incubation time, the more NPs eluted into the medium, resulting in lower viability. For all dressings, it was observed that the cytotoxic effect decreased with the dilution of the medium, and no cytotoxic effect was observed at a dilution of 1:4. Detailed results are available in the supplementary material (see the *Supplementary document* – Figure S2 for further details regarding these results).

In conclusion, the safety and efficiency testing showed that the dressing itself provides a suitable environment for skin fibroblasts and HaCaT cells and can be used on the skin without causing a cytotoxic effect. At the same time, the addition of NPs at a concentration of 0.5 wt % or higher is sufficient to kill melanoma cells. In Fig. 6E, we show an application scenario in which the outer side of the dressing does not contain NPs and protects healthy skin, while the inner side of the dressing contains NPs that have a cytotoxic effect on melanoma cells. Whereas this hypothesis is applicable in practice in such a form was not directly tested in the scope of this article. However, such a formulation is easily prepared in a controlled manner using 3D printing. Namely, this technique can be used to create a carefully modified dressing that can adapt to any melanoma in terms of size and shape. 3D printing technology can achieve any shape and size, allowing for personalized topical melanoma treatment. By conforming to the shape of the diseased tissue, 3D printed dressings can maximize efficacy while minimizing side effects on healthy tissue. Considering the positive overall results of safety and efficiency testing using cells, we can claim that such dressings have a high potential for further testing towards clinical application.

To potentially shed further light on the influence of the nanoparticle-loaded materials on the healthy and malignant cells, the viability of skin fibroblasts and HaCaT cells was evaluated after incubation with dressings with added NiCu NPs. In contrast, the viability of malignant melanoma cells was measured after incubation with the dressing without NPs (see the *Supplementary document* – Figure S1 for further details regarding these results). Briefly, NPs loaded particles also negatively influenced the healthy cell viability, whereas the formulation without added NPs did not negatively influence the growth of melanoma cells. This result further backs the idea shown in Fig. 6D to produce personalized dressings according to specific patient needs.

Cell based testing with NPs: E) Viability of malignant melanoma cells when in contact with dressings extracts incubated in cell media for 24 h F) Viability of malignant melanoma cells when in contact with dressings extracts incubated in cell media for 72 h.

4. Conclusions

In this work, novel 3D printed dressings with customizable composition and geometry were developed for potential antimelanoma applications. The results show that alginate – methyl cellulose – nanofibrilated cellulose composite hydrogel supplemented with NiCu nanoparticles (NiCu NPs) enables 3D printing of customizable dressings with tailored geometric, structural, and surface characteristics. Extracts from 3D printed scaffolds supplemented with NiCu NPs significantly decreased melanoma cell viability, while the base material (without NPs) had a positive effect on the two most abundant skin cells, keratinocytes (from the epidermis, which is directly exposed to topical formulations) and fibroblasts (the main cell type in the dermis, which get exposed after prolonged exposures in non-wounded skin or immediately in case of wounds). By adjusting the structural and chemical composition and customizing their geometry using 3D printing, patient-specific dressings can be made to stop the progression of cancerous tissue and stimulate the growth of surrounding healthy cells. By matching the shape of the diseased tissue, precisely manufactured dressings can maximize efficacy while minimizing side effects, which, as demonstrated in this work, is possible with the proposed production design. Although further testing will be required to fully demonstrate the potential of the developed dressing for targeted topical melanoma therapies, we believe the results already suggest that this next step is reasonable.

Credit author statement

Laura Činč Ćurić: Conceptualization, Formal analysis, Investigation Methodology, Writing - Original Draft, Visualization. **Maša Šuligoj:** Conceptualization, Formal analysis, Investigation Methodology, Writing - Original Draft, Visualization. **Maja Ibic:** Conceptualization, Formal analysis, Investigation Methodology, Writing - Original Draft, Visualization. **Nina Marovič:** Conceptualization, Formal analysis, Investigation Methodology, Writing - Original Draft, Visualization. **Boštjan Vihar:** Conceptualization, Formal analysis, Writing - Review & Editing. **Matej Vesenjak:** Methodology, Formal analysis, Visualization. **Polona Dobnik Dubrovski:** Methodology, Formal analysis, Visualization. **Nejc Novak:** Methodology, Investigation. **Janja Stergar:** Methodology, Investigation. **Irena Ban:** Methodology, Investigation. **Uroš Maver:** Conceptualization, Writing - Review & Editing, Supervision, Project administration, Resources, Funding acquisition. **Marko Milojević:** Conceptualization, Formal analysis, Writing - Review & Editing, Supervision, Project administration. **Tina Maver:** Conceptualization, Writing - Review & Editing, Supervision, Project administration, Resources, Funding acquisition.

Declaration of competing interest

The authors declare that they have no known competing financial interests or personal relationships that could have appeared to influence the work reported in this paper.

Data availability

Data will be made available on request.

Acknowledgements

The authors acknowledge the financial support for this study received from the Slovenian Research and Innovation Agency (grant numbers: P3-0036, I0-0029, L7-4494, J3-1762 and Z3-4529) and through the Young Researcher Programme.

Appendix A. Supplementary data

Supplementary data to this article can be found online at https://doi.org/10.1016/j.mtbio.2023.100770.

References

[1] Y. Li, D. Ye, M. Li, M. Ma, G. Ning, Adaptive materials based on iron oxide nanoparticles for bone regeneration, ChemPhysChem 19 (2018).
[2] M. Milojević, L. Gradišnik, J. Stergar, M. Skelin Klemen, A. Stožer, M. Vesenjak, P. Dobnik Dubrovski, T. Maver, T. Mohan, K. Stana Kleinschek, U. Maver, Development of multifunctional 3D printed bioscaffolds from polysaccharides and NiCu nanoparticles and their application, Appl. Surf. Sci. 488 (2019) 836–852.
[3] C. Dannert, B.T. Stokke, R.S. Dias, Nanoparticle-hydrogel composites: from molecular interactions to macroscopic behavior, Polymers 11 (2) (2019).
[4] T. Maver, T. Mastnak, M. Mihelič, U. Maver, M. Finšgar, Clindamycin-based 3D-printed and electrospun coatings for treatment of implant-related infections, Materials 14 (6) (2021) 1464.
[5] T. Zidaric, M. Milojevic, L. Gradisnik, K. Stana Kleinschek, U. Maver, T. Maver, Polysaccharide-based bioink formulation for 3D bioprinting of an in vitro model of the human dermis, Nanomaterials 10 (4) (2020).
[6] S.N. Patel, M. Ishahak, D. Chaimov, A. Velraj, D. LaShoto, D.W. Hagan, P. Buchwald, E.A. Phelps, A. Agarwal, C.L. Stabler, Organoid microphysiological system preserves pancreatic islet function within 3D matrix, Sci. Adv. 7 (7) (2021).
[7] M. Milojević, B. Vihar, L. Banović, M. Miško, L. Gradišnik, T. Zidarič, U. Maver, Core/shell printing scaffolds for tissue engineering of tubular structures, JoVE 151 (2019), e59951.
[8] S.K. Schmidt, R. Schmid, A. Arkudas, A. Kengelbach-Weigand, A.K. Bosserhoff, Tumor cells develop defined cellular phenotypes after 3D-bioprinting in different bioinks, Cells 8 (10) (2019) 1295.
[9] L. Cheng, B. Yao, T. Hu, X. Cui, X. Shu, S. Tang, R. Wang, Y. Wang, Y. Liu, W. Song, X. Fu, H. Li, S. Huang, Properties of an alginate-gelatin-based bioink and its potential impact on cell migration, proliferation, and differentiation, Int. J. Biol. Macromol. 135 (2019) 1107–1113.
[10] P. Rastogi, B. Kandasubramanian, Review of alginate-based hydrogel bioprinting for application in tissue engineering, Biofabrication 11 (4) (2019), 042001.
[11] M. Kristl, I. Ban, S. Gyergyek, U. Maver, J. Stergar, Sol–gel preparation of NixCu1–x/silica nanocomposites using different silica precursors, J. Sol. Gel Sci. Technol. 101 (2022).
[12] I. Ban, J. Stergar, U. Maver, NiCu magnetic nanoparticles: review of synthesis methods, surface functionalization approaches, and biomedical applications, Nanotechnol. Rev. 7 (2) (2018) 187–207.
[13] J. Chatterjee, M. Bettge, Y. Haik, C. Jen Chen, Synthesis and characterization of polymer encapsulated Cu–Ni magnetic nanoparticles for hyperthermia applications, J. Magn. Magn Mater. 293 (1) (2005) 303–309.
[14] A. Kuznetsov, V. Leontiev, V. Brukvin, G. Vorozhtsov, B. Kogan, O. Shlyakhtin, A. Yunin, O. Tsybin, O. Kuznetsov, Local radiofrequency-induced hyperthermia using CuNi nanoparticles with therapeutically suitable Curie temperature, J. Magn. Magn Mater. 311 (2007) 197–203.
[15] P. Amrollahi, A. Ataie, A. Nozariasbmarz, E. Seyedjafari, A. Shafiee, Cytotoxicity evaluation and magnetic characteristics of mechano-thermally synthesized CuNi nanoparticles for hyperthermia, J. Mater. Eng. Perform. 24 (2015).
[16] J. Stergar, I. Ban, U. Maver, The potential biomedical application of NiCu magnetic nanoparticles, Magnetochemistry 5 (4) (2019) 66.
[17] J. Stergar, I. Ban, L. Gradisnik, U. Maver, Novel drug delivery system based on NiCu nanoparticles for targeting various cells, J. Sol. Gel Sci. Technol. 88 (2018).
[18] G. Ferk, J. Stergar, M. Drofenik, D. Makovec, A. Hamler, Z. Jagličić, I. Ban, The synthesis and characterization of nickel–copper alloy nanoparticles with a narrow size distribution using sol–gel synthesis, Mater. Lett. 124 (2014) 39–42.
[19] S.J. Bidarra, C.C. Barrias, P.L. Granja, Injectable alginate hydrogels for cell delivery in tissue engineering, Acta Biomater. 10 (4) (2014) 1646–1662.
[20] A.D. Augst, H.J. Kong, D.J. Mooney, Alginate hydrogels as biomaterials, Macromol. Biosci. 6 (8) (2006) 623–633.
[21] J.H. Teoh, F.T. Abdul Shakoor, C.H. Wang, 3D printing methyl cellulose hydrogel wound dressings with parameter exploration via computational fluid dynamics simulation, Pharmaceut. Res. 39 (2) (2022) 281–294.
[22] A.G. Dumanli, Nanocellulose and its composites for biomedical applications, Curr. Med. Chem. 24 (5) (2017) 512–528.
[23] J. Vajda, B. Vihar, L.Č. Ćurić, U. Maver, M. Vesenjak, P.D. Dubrovski, M. Milojević, Sr2+ vs. Ca2+ as post-processing ionic crosslinkers: implications for 3D bioprinting of polysaccharide hydrogels in tissue engineering, J. Mater. Res. Technol. 23 (2023) 1805–1820.
[24] B. Vihar, J. Rožanc, B. Krajnc, L. Gradišnik, M. Milojević, L. Činč Ćurić, U. Maver, Investigating the viability of epithelial cells on polymer based thin-films, Polymers 13 (14) (2021) 2311.
[25] Y. Zhang, L. Ye, J. Cui, B. Yang, H. Sun, J. Li, F. Yao, A biomimetic poly (vinyl alcohol)–carrageenan composite scaffold with oriented microarchitecture, ACS Biomater. Sci. Eng. 2 (4) (2016) 544–557.
[26] M. Kurečič, T. Maver, N. Virant, A. Ojstršek, L. Gradišnik, S. Hribernik, M. Kolar, U. Maver, K.S. Kleinschek, A multifunctional electrospun and dual nano-carrier biobased system for simultaneous detection of pH in the wound bed and controlled release of benzocaine, Cellulose 25 (12) (2018) 7277–7297.
[27] U. Maver, K. Xhanari, M. Žižek, D. Korte, L. Gradišnik, M. Franko, M. Finšgar, A combination of interdisciplinary analytical tools for evaluation of multi-layered coatings on medical grade stainless steel for biomedical applications, Eur. J. Pharm. Biopharm. 128 (2018) 230–246.
[28] M. Ferrari, M.C. Fornasiero, A.M. Isetta, MTT colorimetric assay for testing macrophage cytotoxic activity in vitro, J. Immunol. Methods 131 (2) (1990) 165–172.
[29] T. Mosmann, Rapid colorimetric assay for cellular growth and survival: application to proliferation and cytotoxicity assays, J. Immunol. Methods 65 (1–2) (1983) 55–63.
[30] N. Eswaramoorthy, D.R. McKenzie, Plasma treatments of dressings for wound healing: a review, Biophysical reviews 9 (6) (2017) 895–917.
[31] L. Cui, Y. Yao, E.K.F. Yim, The effects of surface topography modification on hydrogel properties, APL Bioeng. 5 (3) (2021), 031509.
[32] G. Ferk, J. Stergar, D. Makovec, A. Hamler, Z. Jagličić, M. Drofenik, I. Ban, Synthesis and characterization of Ni–Cu alloy nanoparticles with a tunable Curie temperature, J. Alloys Compd. 648 (2015) 53–58.
[33] F. Fan, S. Saha, D. Hanjaya-Putra, Biomimetic hydrogels to promote wound healing, Front. Bioeng. Biotechnol. 9 (2021), 718377.
[34] S. Wang, W.-Y. Wu, J.C.C. Yeo, X.Y.D. Soo, W. Thitsartarn, S. Liu, B.H. Tan, A. Suwardi, Z. Li, Q. Zhu, X.J. Loh, Responsive Hydrogel Dressings for Intelligent Wound Management, 2021. BMEMat n/a(n/a) e1.
[35] Y. Jiang, N. Krishnan, J. Heo, R.H. Fang, L. Zhang, Nanoparticle-hydrogel superstructures for biomedical applications, J. Contr. Release 324 (2020) 505–521.
[36] M. Milojević, G. Harih, B. Vihar, J. Vajda, L. Gradišnik, T. Zidarič, K. Stana Kleinschek, U. Maver, T. Maver, Hybrid 3D printing of advanced hydrogel-based wound dressings with tailorable properties, Pharmaceutics 13 (4) (2021) 564.
[37] A.K. Gaharwar, N.A. Peppas, A. Khademhosseini, Nanocomposite hydrogels for biomedical applications, Biotechnol. Bioeng. 111 (3) (2014) 441–453.
[38] M. Milojević, J. Rožanc, J. Vajda, L. Činč Ćurić, E. Paradiž, A. Stožer, U. Maver, B. Vihar, In Vitro Disease Models of the Endocrine Pancreas 9 (10) (2021) 1415.